JOURNAL OF OCULAR PHARMACOLOGY AND THERAPEUTICS
Volume 32, Number 5, 2016

DOI: 10.1089/jop.2015.0157

Nanofiber Scaffold-Based Tissue-Engineered Retinal Pigment Epithelium to Treat Degenerative Eye Diseases

Nathan A. Hotaling,[1,2] Vladimir Khristov,[3] Qin Wan,[3] Ruchi Sharma,[2] Balendu Shekhar Jha,[2] Mostafa Lotfi,[3] Arvydas Maminishkis,[3] Carl G. Simon Jr.,[1] and Kapil Bharti[2]

Abstract

Clinical-grade manufacturing of a functional retinal pigment epithelium (RPE) monolayer requires reproducing, as closely as possible, the natural environment in which RPE grows. *In vitro*, this can be achieved by a tissue engineering approach, in which the RPE is grown on a nanofibrous biological or synthetic scaffold. Recent research has shown that nanofiber scaffolds perform better for cell growth and transplantability compared with their membrane counterparts and that the success of the scaffold in promoting cell growth/function is not heavily material dependent. With these strides, the field has advanced enough to begin to consider implementation of one, or a combination, of the tissue engineering strategies discussed herein. In this study, we review the current state of tissue engineering research for *in vitro* culture of RPE/scaffolds and the parameters for optimal scaffold design that have been uncovered during this research. Next, we discuss production methods and manufacturers that are capable of producing the nanofiber scaffolds in such a way that would be biologically, regulatory, clinically, and commercially viable. Then, a discussion of how the scaffolds could be characterized, both morphologically and mechanically, to develop a testing process that is viable for regulatory screening is performed. Finally, an example of a tissue-engineered RPE/scaffold construct is given to provide the reader a framework for understanding how these pieces could fit together to develop a tissue-engineered RPE/scaffold construct that could pass regulatory scrutiny and can be commercially successful.

Introduction

The retinal pigment epithelium (RPE) is a light-absorbing monolayer of cells in the back of the eye that is crucial for retinal function. RPE cells interact with light-sensing photoreceptor outer segments, providing ion, nutrient, fluid, and metabolite transport, polarized secretion of cytokines, and promote homeostasis between the photoreceptor and the choroid.[1–3] RPE also recycles the visual pigment, retinal, which is a key intermediary in the visual cycle.[4] Due to this extensive interaction between the RPE and the photoreceptors, deficits in RPE function often manifest as problems with vision. For example, in age-related macular degeneration, a regional atrophy of RPE precedes vision loss[5] or forms of retinitis pigmentosa where RPE pathology leads to vision loss.[6]

In healthy eyes, RPE cells are found on a dense layer of proteins, glycosaminoglycans, and signaling molecules known as Bruch's membrane. The backbone structure of this membrane primarily comprises collagen I–V, laminin, and fibronectin.[7] The fibers of Bruch's membrane range from $\sim$50 to 500 nm in diameter and the membrane is <5 μm thick.[7] Over the lifetime, an individual Bruch's membrane is maintained by RPE cells.[8] The membrane is thought to help RPE cells maintain their monolayer structure and maintain sufficient hydraulic conductivity for free-flow of nutrients and metabolites to and from the choriocapillaris that is situated on the other side of Bruch's membrane.[8–11] In addition, a basal support membrane has been shown to be critical to long-term RPE survival after implantation.[12] Thus, it is thought that tissue engineering strategies that enable RPE to grow on a fibrous/permeable supporting scaffold that is similar to Bruch's membrane while also enabling the RPE to grow and develop in a mechanically robust monolayer for transplantation will likely provide a successful therapy for RPE-associated retinal degenerative disorders.[12,13]

Multiple approaches are being tested for growth of an RPE monolayer.[14,15] A popular approach is to use scaffolds

[1]Biosystems and Biomaterials Division, National Institute of Standards and Technology, Gaithersburg, Maryland.
[2]Unit on Ocular and Stem Cell Translational Research and [3]Section of Epithelial and Retinal Physiology and Disease, National Eye Institute, National Institutes of Health, Bethesda, Maryland.

as a substrate for RPE culture. Scaffold substrate culture of RPE can be divided along natural,[16–18] synthetic,[19–21] or hybrid[16] fiber formulations (Jha and Bharti[15] provide a comprehensive list of different kinds of scaffold approaches that have been tested in preclinical and clinical studies). In this study, natural scaffolds[22] are defined as scaffolds whose components are derived from biological sources, synthetic nondegradable[23] and synthetic degradable poly-L-lactic acid (PLLA), poly(lactic-co-glycolic acid) (PLGA), polycaprolactone (PCL), etc.] scaffolds[24–26] are defined as those whose constituents are inorganic in derivation, and hybrid scaffolds are defined as those that contain elements of both natural and synthetic scaffolds.

In comparisons between membrane and fibrous scaffolds, it has been found that fibrous substrates are more similar in 3-dimensional (3D) structure to Bruch's membrane and enhance RPE function and viability regardless of formulation.[14,24,27] Thus, the focus of this review is on nanofiber scaffolds and recent developments that indicate specific design requirements for either natural or synthetic scaffolds, which dramatically improve translational likelihood of RPE on nanofibrous scaffolds. In this review, we focus on nanofibrous scaffolds for RPE transplantation. However, several recent publications have shown promising results using nonfibrous membrane approaches.[12,13,23,28,29] For example, Lu et al. created submicron parylene-C membranes and found that 0.15–0.30 μm membranes had similar permeability to healthy human Bruch's membranes and that RPE cells grown on them were able to form tight junctions and become well polarized with microvilli.[23] These membrane studies have shown promising results, but are outside the scope of this review.

In the first part of this review, we focus on characterization of RPE, natural, and hybrid scaffolds. We note that both natural and hybrid scaffolds are limited in their potential to provide a commercially scaled-up, consistently manufactured, regulatory approved product. In the second part of this review, we review manufacturing, characterization, and scale-up challenges associated with synthetic polymer-based nanofiber scaffolds and compare them with natural and hybrid scaffolds. In the last part of the review, we provide data on our efforts to grow and characterize induced pluripotent stem cell (iPSC)-derived RPE on nanofiber scaffolds and discuss the relevance of nanofiber scaffolds for clinical application.

Generation and Characterization of RPE Cells

In the case of degenerative diseases, cell replacement therapy that leads to replacement of diseased cells by healthy cells is an attractive treatment option. This approach is particularly intriguing for degenerative eye diseases that involve the RPE because it has been shown that replacement of damaged/diseased RPE can mitigate vision loss.[30,31] Recent advances in the differentiation of RPE cells from embryonic stem (ES) cells and iPSCs have opened up the possibility for a commercial-grade cell replacement therapy for these degenerative eye diseases.[32,33] Although both ES and iPSC sources can be used for the cell replacement therapy, iPSCs provide an autologous and immune-compatible source of cells for patients without ethical concerns.[34]

iPSCs can be reproducibly differentiated into RPE cells using a previously described protocol.[35] To drive neural induction of iPSCs, they are transferred to knockout serum replacement (KSR) medium supplemented with NOGGIN and SB431542, 2 inhibitors of the TGF-beta pathways.[36] After 5 days of neural induction, RPE fate is specified by adding nicotinamide and Activin A to the KSR medium. Characteristic RPE colonies with hexagonal cell shape and pigmentation appear between 3 and 5 weeks. Figure 1 shows several steps of the differentiation process starting with iPSCs aggregated into embryoid bodies (Fig. 1A). An intermediate stage of committed, but not yet functional, RPE can be seen in Fig. 1B after a week of differentiation. After maturation and differentiation are complete, RPE cells demonstrate specific expression of tight junction marker ZO-1 (green), hexagonal morphology (Fig. 1C, D), and abundant apical processes (Fig. 1D). The enriched RPE monolayer can then be maintained for long periods in RPE medium.[37]

To be considered for cell therapy, iPSC-derived RPE must recapitulate native RPE functionality. Native RPE is characterized by a variety of molecular and physiological traits, including abundant apical processes, hexagonal cell shape, mature tight junctions, basal enfoldings, and apical localization of the melanosomes,[38] as seen by a scanning electron microscope (SEM)/transmission electron microscope. Additionally, RPE shows high expression of functional markers, such as TTR, RPE65, E-CADHERIN, CLAUDIN 19, EZRIN, ZO-1, MERTK, BEST1, and CHI3L1[37,39–41]; polarized secretion of vascular endothelial growth factor (VEGF), pigment epithelium-derived factor (PEDF), and other cytokines[11]; a transmembrane resistance >400 $\Omega \cdot cm^2$;[11] a transmembrane potential of 3–5 mV, ability to phagocytose photoreceptor outer segments; and ability to pump fluid transepithelially at a rate of $\sim 5\,\mu L/h$ per cm^2.[11]

The above protocols and cell characteristics are a brief summary of typical traits of RPE. However, a full description of the body of work that has been completed toward the generation and characterization of RPE is outside the purview of this report and has been covered in more detail in several publications[15,42] and thus will not be discussed in further detail here.

RPE Culture on Nanofibrous Scaffolds

Natural scaffolds

Natural RPE scaffolds such as native Bruch's membrane explants, amniotic membrane, and collagen nanofibers have the advantage of being as close to native tissue as is currently possible to achieve. These scaffolds have nanofibers that closely match the natural physiological properties of Bruch's membrane in several key areas: concentration of protein, mechanical properties, morphological properties, and biocompatibility. These fibrous membranes' similarity to native Bruch's membrane makes them promising candidates for clinical translation.

In earlier studies, RPE cells were cultured on explants of human Bruch's membrane or its constituent layers.[22,43–47] These studies found that the basal layer of Bruch's membrane, which consists of mostly collagen IV α3-5 and laminins,[7] was critical to RPE survival, proliferation, and function.[44,47] Other layers of human Bruch's membrane were also found to support RPE growth, but the level of

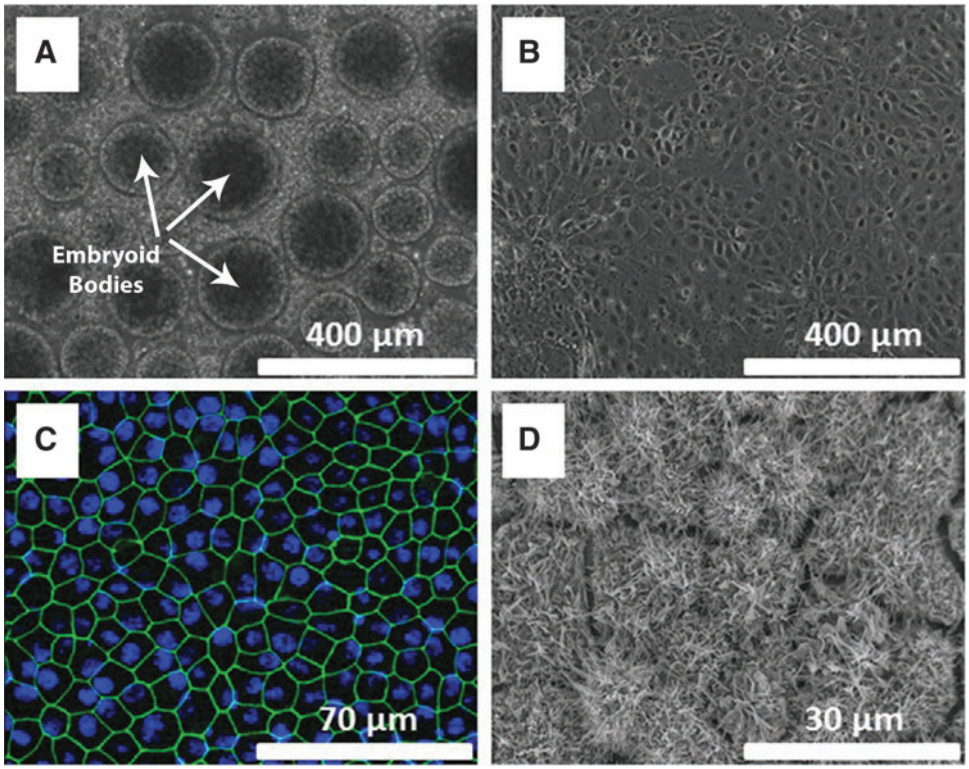

FIG. 1. Derivation of RPE cells from iPSCs. iPSCs aggregated into embryoid bodies (*arrows* show a few embryoid bodies of the many in the image) at the start of differentiation **(A)**. Committed RPE cells that have not yet developed RPE morphology after 1 week of culture **(B)**. Mature iPSC-derived RPE cells demonstrate hexagonal morphology similar to that of native tissue after 5 weeks in culture transwell membrane, expressing the tight junction marker ZO-1 (*green*) with the nucleus of the RPE stained with DAPI (*blue*) **(C)**. Scanning electron micrograph of mature iPSC-RPE cells after 5 weeks in culture on the scaffold with each cell projecting abundant apical processes as shown by the small rods and tongues protruding from each cell surface **(D)**. iPSC, induced pluripotent stem cell; RPE, retinal pigment epithelium.

support decreased in direct relation to the distance of the layer from the basal lamina of the RPE.[44,47] Similarly, in explants of aged Bruch's membrane, it was found that RPE had impaired survival that was correlated with decreased prevalence of typical basal layer proteins.[43,45,46] Later, it was found that some of the RPE's natural functionality could be recovered by either reengineering the lower layers of Bruch's membrane or aged Bruch's membrane to include more laminin and other extracellular matrix (ECM) proteins[46,48,49] or to give cells seeded on these membranes a soluble factor derived from conditioned media by bovine corneal endothelial cells to aid in the resurfacing of Bruch's membrane.[50] However, due to the limited supply of Bruch's membrane available for transplantation and its impaired ability to support RPE growth when derived from elderly donors,[44] it has not been pursued as a possible source for clinical-grade applications.

Human amniotic membrane is another fibrous tissue that has been used as a replacement for Bruch's membrane.[51–54] Human amniotic membrane has been shown to support RPE growth and functionality.[51,53] Akrami et al. showed that RPE grown on amniotic membranes expresses higher levels of the RPE genes, *RPE65*, *CRALBP*, *BESTROPHIN*, and tyrosinase-related protein *(TRP)-2*, compared with cells cultured in traditional tissue culture plates.[52,55] Additionally, protein production of commonly secreted RPE proteins, VEGF, thrombospondin-1, and PEDF, increased in cells cultivated on amniotic membranes.[53] In another study, the transepithelial electrical resistance (TER) of the RPE cells cultured on human amniotic membrane was measured and found to be significantly higher at 4 weeks of culture compared with cells not grown on the amniotic membrane.[55] Similarly, another naturally derived tissue, porcine lens capsule, has been shown to promote RPE growth leading to pigmented hexagonal morphology.[14,56]

Nanofiber scaffolds have also been fabricated from collagen[18] and bacterial cellulose[17] for use with RPE cells. While these scaffolds were not natural, in that both the collagen and bacterial cellulose scaffolds were created from monomeric proteins and not direct explants of tissues, the base material for these scaffolds was biologically derived and thus considered natural here. Acetylated bacterial cellulose showed high initial RPE adhesion and supported RPE growth and proliferation.[17] Similarly, collagen fiber films supported the growth, maturation, and viability of human embryonic stem cell-derived RPE (hESC-RPE) cells.[18] Collagen I and IV were used in this study and it was found that transepithelial resistance, surface protein expression, growth factor secretion, and phagocytic activity of the hESC-RPE cells matched more closely to that of native RPE than of cells grown on tissue cultured polystyrene.[18] Collagen I/IV films used by Sorkio et al. were created using Langmuir–Schaefer deposition, an industrial scalable technique in which multilaminar films can be produced through creation of thin films on immiscible

liquid surfaces.[18] Therefore, these films are considered translatable to a commercial-scale industrial process. However, there is significant variability in sources for collagen[57] compared with fully synthetic scaffolds and thus the latter would be preferable for clinical applications.

Hybrid scaffolds

Hybrid scaffolds have the potential to combine the properties of both natural and synthetic nanofibers, creating a scaffold with all of the advantages of a natural scaffold in terms of protein composition and native appearance and the tailorability of synthetic scaffolds. However, the use of biologically derived proteins/structures could lead to potential hurdles for ultimate regulatory approval as variability of bulk biologically derived materials is known to vary based on the source and the time postisolation.[57] Xiang et al. created a hybrid scaffold that was a combination of Antheraea pernyi silk fibroin (RWSF), PCL, and gelatin (Gt).[16] The fibers were engineered to have a mean diameter of 165 ± 85 nm, which is the approximate size that Liu et al.[58] found to be optimal for RPE cell growth. Human RPE cells seeded on the RWSF/PCL/Gt nanofiber scaffolds showed a higher cell growth rate than did tissue culture plastic or PCL fibers alone. Additionally, cells grown on these hybrid fibers showed a typical expression pattern of RPE signature genes (*CRALBP, PEDF, VEGF, MITF,* and *PMEL* 17 among others), enhanced expression of secreted factors, and reduced expression of inflammatory mediators.[16] In addition, within 12 weeks of cultivation, the RPE on the hybrid scaffolds had polygonal morphology, was able to phagocytose porcine photoreceptor outer segments, and had developed apical microvilli.[16] Finally, the hybrid scaffolds were implanted into the subsclera intraocular space and the membranes were well tolerated without inflammation of the choroid or the retina.[16] This study shows the promise of hybrid scaffolds, but future work remains in characterization of the cells and scaffolds to ensure reproducibility of the approach to achieve optimal clinical and commercial-scale manufacturing.

Synthetic nanofibrous scaffolds

Synthetic nanofiber scaffolds have the advantage of being able to have characteristics such as well-defined and xeno-free constituents, tailorable fiber diameter, porosity, and hydrophilicity. Additionally, synthetic fibers have the advantage that the nanofiber surface properties can be easily modified in a defined and controlled way. The consistency and tailorability of synthetic materials are perhaps the 2 key factors that make them a promising candidate for clinical translation. Multiple different types of synthetic scaffolds (fibrous and nonfibrous polymeric) have been used for RPE culture and are being tested as potential scaffolds for transplantation in patients. In this study, we briefly summarize previous and ongoing work using RPE and synthetic scaffolds and review in depth the manufacturing, characterization, and use of nanofibrous scaffolds for RPE culture.

Unmodified nanofiber surfaces have been shown to promote RPE growth over that of smooth, plastic nonporous membranes or glass culture surfaces.[27,58] Unmodified poly(D-L-lactic acid) (PDLLA) nanofibers supported by a poly(4-dioxanone) frame were shown to improve RPE tight junction formation, promote a hexagonal morphology of the RPE, and increase expression of RPE65 over that of PDLLA films.[25] When transplanted into the subretinal space of a porcine eye and then removed, the construct was shown to maintain cell viability and could be easily implanted as an unfolded monolayer.[25] However, cells grown on the PDLLA nanofibrous membranes were only able to produce relatively low TER of $179 \pm 59\ \Omega \cdot cm^2$ after 1 month in culture. Thus, physiological functionality of these tissue-engineered constructs is unclear. Liu et al. also showed that either polyethylene terephthalate (PET) or poly(L-lactide-co-ε-caprolactone) (PLCL)-uncoated nanofiber scaffolds were able to promote functional RPE growth over that of films.[58] RPE was assessed for attachment, growth, pigmentation, and tight junction formation. In all measured outputs, RPE on nanofibers with a mean diameter of 200 nm had the highest performance, regardless of starting material.[58] However, the nanofiber scaffolds studied by Liu et al. were not rigid enough to transplant into the subretinal space without a mechanical support and thus transplantations into rabbit eyes were performed with the scaffolds attached to porous PET membranes. The PET membranes, while showing good initial incorporation into native tissue,[58] are not biodegradable and have limited porosity, which could eventually inhibit functionality of the tissue-engineered construct.

To address this concern, Warnke et al. chose scaffolds that were only made from PLGA or type I collagen.[24] RPE attachment, proliferation, phagocytosis of latex beads, and surface marker expression were measured on both scaffolds and compared with PLGA and collagen films. It was found that either fiber formulation supported RPE attachment, growth, and the ability of the RPE to phagocytose latex beads. Furthermore, polygonal morphology of the cells was higher on either of the nanofiber samples than on the films. However, no *in vivo* transplantation of these cell/scaffolds was performed and thus the mechanical robustness of the scaffolds and the viability of the cells post-transplantation are unknown.

Surface modification of nanofibers has been shown to have larger synergistic benefits compared with seeding RPE onto nanofibers alone.[19,20,26] For example, polytetrafluoroethylene fibrous membranes were modified with ammonia gas plasma treatments, which were shown to enhance protein adhesion and improve RPE attachment, formation of tight junctions, and increase phagocytosis of photoreceptor outer segments.[20] In a similar study, in which cell attachment molecules, RGD and YIGSR, were attached to the backbone of polyamide fibers, RPE was shown to improve viability and proliferation over that of polyamide fibers alone and to a similar degree to that of Laminin-coated fibers.[19]

Plasma treatment of fibers and the adsorption of ECM protein collagen IV onto PLCL were also shown to enhance RPE growth and maturation.[59] Cell proliferation assays, RT-PCR, immunostaining of RPE-specific markers, MITF, BESTROPHIN, CRALBP, and ZO-1, and TER measurements, as well as *in vitro* phagocytosis assay, clearly demonstrated that the plasma-treated PLCL scaffolds supported the adherence, proliferation, maturation, and functionality of hESC-RPE cells in serum-free culture conditions to a greater extent than untreated fibers.[59] The trend of enhanced RPE functionality with the adsorption of ECM proteins was further confirmed by Thomson et al. who showed that adsorption of laminin onto PLLA/PLGA polymer blend

nanofiber scaffolds enhanced cell viability and proliferation.[26] The advantage of these coating techniques is that the bulk size and mechanical properties of the nanofiber scaffolds are not altered and thus including them, assuming the coating agents are good manufacturing processing (GMP)-grade and xeno-free materials, only enhances scaffold properties without detracting from the scaffolds' translatability to the clinic.

Clinically Viable, Synthetic Nanofiber Scaffold Fabrication

To implement any of the above discussed nanofiber scaffold technologies, researchers would need to be able to produce nanofiber scaffolds in a reproducible, scalable, regulatory approved manner. The combination of these factors is not trivial, but to meet this need, bioengineers have recently developed manufacturing processes[60,61] that can recapitulate a fibrous ECM-like structure similar to Bruch's membrane, matching fiber size, scale, and approximate mechanical properties at industrial scales. However, even as production has scaled challenges for how to assess batch consistency, a necessity for clinical therapies has arisen and only recently have automated solutions[62,63] begun to be robust enough for feasible studies to be conducted. In this study, we review the production techniques of nanofiber scaffolds that are both industrially and clinically viable, assessment methodologies for nanofiber morphology, and scaffold mechanical properties.

Nanofibers have been created using a variety of methods, including electrospinning,[64,65] melt spinning,[66,67] blow spinning,[68] template synthesis,[69,70] rotary jet spinning,[71] and self-assembly.[72,73] The first and most pervasive technique of nanofiber creation is electrospinning.[74] Traditionally, electrospinning devices contain a high voltage source, which has 1 terminal connected to a single metallic needle through which a polymer dissolved in a solvent is extruded at a constant rate. The ground of the voltage source is then connected to a conductive collector plate, which is placed a set distance from the needle. Figure 2 shows a diagram of an electrospinning device with labels for appropriate equipment and Fig. 3A shows electrospun PLGA fibers that were made using clinical-grade PLGA (50:50; 50% lactide to 50% glycolide composition; Durect Corporation) and an in-house-developed electrospinning device identical to that shown in Fig. 2. Fibers were spun using a PLGA 50:50 polymer with a molecular weight of 119.3 relative molecular mass units dissolved in hexafluoroisopropanol, at a 28 weight percent concentration, using a 21-gauge needle, 12.5 kV potential difference, 0.65 mL/h flow rate, and an 18-cm needle to collector plate distance. All spinning was performed at room temperature with 30% humidity. The large voltage potential difference between the needle and the ground causes the polymer to form a conical body, called a Taylor cone, at the needle tip from which a nanofiber is pulled onto the collector plate through the electromotive force generated by the potential difference.[75] The diameter and rate of formation of the nanofiber depend on a variety of environmental and device-dependent factors, such as humidity, temperature, polymer molecular weight, voltage, and solvent.[75–79] Many in-depth reviews have covered the factors that influence electrospun nanofiber formation and morphology and thus will not be further discussed here.[75–79]

Multineedle and high surface area needleless electrospinning

Classic single-needle electrospinning is not suited for industrial scale production of nanofiber scaffolds due to the small needle gauge necessary to create nanofibers, relatively slow flow rates of polymer extrusion from the needle, and sensitivity of the system to environmental factors. Multineedle spinning is one method that has been used to improve the production efficiency of nanofiber scaffolds. To this end, Tomaszewski and Szadkowski[80] showed that by altering the configuration of needles and the distance between needles, researchers could drastically affect the nanofiber scaffold produced. Linear, elliptic, and concentric needle configurations were used and it was shown that both elliptic and concentric needle layouts were able to produce nanofibers efficiently and that nanofiber production scaled linearly with the number of needles used in the system. These findings have led to commercial systems in which 1,000 nozzle arrays are able to produce industrial-scale nanofiber scaffolds.[81]

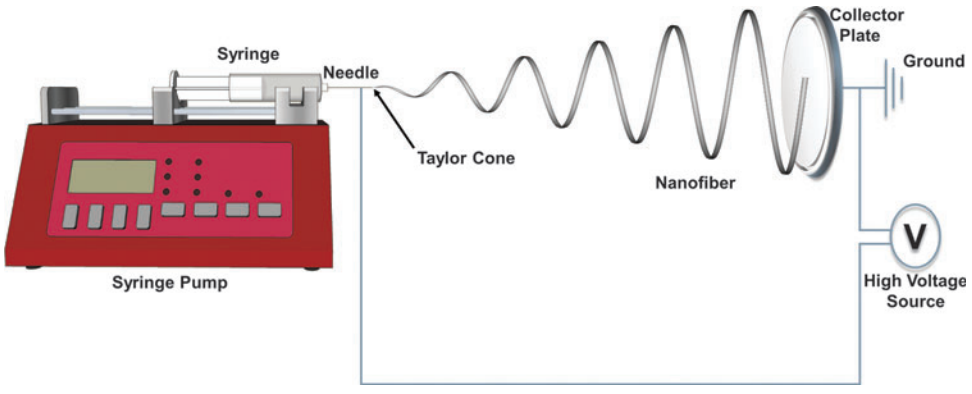

FIG. 2. Schematics of electrospinning workflow. A syringe pump pushes polymer from the syringe out through the needle. The needle is connected to a high voltage source whose ground is attached to a metallic collector plate. While extruding the polymer, the high voltage source is turned on. The electromotive force generated between the needle tip and the collector plate causes a Taylor cone to form at the needle tip, from which a nanofiber is extruded. The nanofiber whips around in a roughly helical pattern until it connects with the collector plate. Nanofibers are collected on the collector plate until the nanofiber mat has reached the desired thickness.

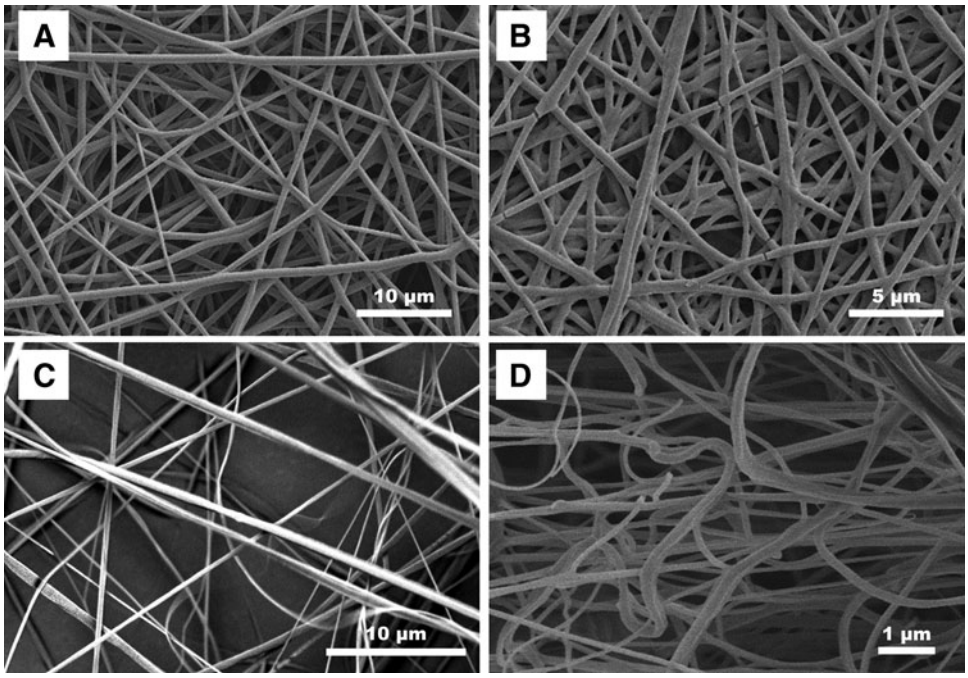

FIG. 3. Comparison of PLGA nanofibers spun using traditional single-needle electrospinning **(A)**, needleless electrospinning **(B)**, rotary jet melt spinning **(C)**, and solution blow spinning **(D)**. PLGA, poly(lactic-co-glycolic acid).

These studies have led to a commercial company, known as Inovenso,[61] which produces both research and industrial-scale nanofiber production equipment.

Needleless electrospinning involves the formation of multiple Taylor cones over a surface without the need for the creation of specific needles or Taylor cone sites.[82–84] Two industrial manufacturers of needleless electrospun scaffolds are SNC Nanofiber Company and Elmarco Incorporated. SNC Nanofiber Company uses a charged rotating electrode sphere, the bottom of which is immersed in a polymer solution, to spin nanofibers. When the sphere is rotated, a thin polymer layer forms on the surface of the sphere and numerous Taylor cones are formed when a strong electrostatic field is placed on the sphere.[85] Similarly, Elmarco developed a system that uses a wire and fluid handler to coat the wire with dissolved polymer before application of an electrostatic field. After the field is applied, Taylor cones form *ad hoc* along the length of the wire and nanofiber production is increased exponentially over single-needle arrays. Morphologically, scaffolds produced by classic single-needle electrospinning look very similar to scaffolds commercially produced through needleless electrospinning as can be seen in Fig. 3B, in which PLGA nanofibers were spun by SNC Nanofiber Company and their needleless electrospinning apparatus.

Rotary jet melt spinning

Using electrostatic potential differences to drive the formation of nanofibers has limitations if the solvent used to dissolve the polymer is cytotoxic. Rotary jet melt spinning was developed to help address this concern. In this method, a polymer is brought to just above its melting temperature and while in this melt state is extruded through a spinneret—similar to how cotton candy is manufactured. The diameter of the extruded fibers is reduced by increasing the shear forces applied per unit area on the extruded polymer jet, which is achieved by increasing the speed that the rotary jet is spun or by reducing the size of the hole from which polymer is extruded.[71,86] Once extruded out of the spinner, the polymer solution solidifies because of rapid cooling from air flow around the fiber.[87] FibeRio Technology Corporation[88] uses centrifugal forces and multiple configurations of porous extrusion surfaces to spin polymer melts and solutions[89] and produces both research and industrial-grade equipment. The main industrial advantage of melt spinning technology relies on the capability to easily spin multicomponent systems and on the absence of solvents during processing, improving environmental safety and enabling a wider variety of biomedical applications.[61] Polylactic acid fibers produced using rotary jet melt spinning can be seen in Fig. 3C. These fibers are morphologically similar, although not identical, to electrospun fibers as can be seen by comparing Fig. 3A, B with C.

Solution spinning

Solution spinning is based on the same principles of melt spinning, but uses polymers dissolved in solvents rather than melting the polymer. Solution spinning can be divided into 2 main fields: dry and wet. In dry spinning, fibers are formed by using air or other inert gases to evaporate the solvent from a stock polymer solution that is being rapidly extruded from an orifice. One of the most important parameters affecting the morphology of dry-spun fibers is the solvent composition. Generally, for solution-spun fibers to form, solvents must have high volatility and low vapor pressure.[90–92] Solution spinning of polymer fibers has been scaled to industrial levels for several materials, including cellulose acetate, acrylic/Orlon, polyvinylchloride, and polyurethane/Lycra.[93] The scaffold shown in Fig. 3D was produced using an in-house-developed solution blow spinning device as outlined by Tutak et al.[94] These fibers were created using a solution of 12% (w/w) PDLLA (Resomer; Sigma Aldrich) in acetone with an air pressure of $\sim$15 psi air at 30 SCFH, with a nozzle diameter of 0.55 mm and a 22-gauge needle to extrude the polymer solution. Solution blow spun scaffold morphology appears to

have less fiber orientation than do the other spinning methods; however, the 3D spatial orientation and density of fibers have not been assessed for any of these methodologies and thus quantitative statements about fiber distribution and orientation cannot be made.

In wet spinning, the polymer solution is extruded in a viscous fluid medium in which the polymer is insoluble, but which is miscible with the spinning solvent. Exchange between solvent and nonsolvent causes phase separation, rapidly removing solvent from the spun filaments and causing fibers to form through precipitation. The solidification involves mass transfer through the polymeric solution–nonsolvent interface, which can lead to defects, such as voids and cross-shape irregularities.[95,96] However, with careful design, this can also lead to creation of defined lengths of polymeric nanofibers.[97,98] Harnessing this strength, Xanofi has created polymer filaments, which have tightly dispersed lengths and diameters ranging from 100 nm to 5 mm.[99]

Nanofiber Scaffold Characterization

Nanofiber scaffolds can be tested for reproducibility using 2 different classes of analysis: morphological and mechanical. Traditionally, measurement of both these elements is less straightforward in nanofiber scaffolds compared with the traditional woven or fiber-based materials because nanofiber diameter is too small for traditional light microscopic techniques; there is inherent variability in nanofiber diameter; fiber orientation is random and nonwoven; mechanical tests at the size scale that the scaffolds would be used in ($<10\,mm^2$) are not standardized; and those tests that are used on samples of this size are typically laborious. However, recently, software and equipment have been developed that can expedite the morphological characterization of scaffolds to offer a more precise description of their structure[63]; and mechanical tests for medical meshes have been adapted for nonwoven nanofiber scaffold testing.[100–102]

Morphological characterization

Typically, assessment of nanofiber morphology has been performed manually with people measuring fiber diameter, orientation, and pore sizes in SEM images using online tools in image analysis software such as ImageJ/FIJI (National Institutes of Health, MD).[103–105] To facilitate this analysis, several laboratories have developed additional tools that allow assessment of nanofiber orientation,[106–109] mesh hole size,[104] and nanofiber diameter[109–111] from SEM images. Several of the tools to assess nanofiber orientation and pore size have been validated[106–109,112–115] and are available to the community for free on ImageJ/FIJI. However, only one validated open source tool to assess nanofiber diameter, DiameterJ, has been made available to the community.[63] Several other laboratories have developed tools to assess nanofiber diameter using edge detection algorithms,[110] Radon Transforms,[109] Euclidean distance,[116] or principle component analysis[111] and there are 2 commercially available pieces of software: FiberMetric (Phenom World) and FibreQuant (NanoScaffold Technologies, LLC.).

Both DiameterJ and the commercial software are total analysis packages, in that they assess fiber diameter, pore size, and fiber orientation. Currently, due to the submicron scale of nanofibers, no software packages, open source or commercial, have been developed to assess the 3D structure of nanofiber scaffolds. However, tools are emerging that can assess the 3D structure of nanofiber scaffolds[117] and so it is hoped that soon quantitative 3D data on scaffold morphology will be available.

Pore structures of nanofiber scaffolds cannot be technically defined as pores because they do not have discreet boundaries. Instead, these structures are large, interconnected 3D void spaces. Due to the lack of 3D characterization techniques for nanofiber scaffolds and because these voids have extremely heterogeneous sizes/shapes within 2D slices, 2 bulk characterization techniques are commonly used to assess nanofiber porosity: mercury porosimetry and Brunauer, Emmett, and Teller (BET) surface area measurements.[118–121] In principle, these techniques are able to characterize the void space of nanofiber scaffolds; however, because scaffolds are deformable bodies and polymeric surfaces can adsorb and absorb gasses, the above techniques are approximations of the ground truth and have not yet been validated with 3D microscopy techniques. The techniques and their caveats have been covered in detail in other publications and thus will not be discussed in further detail here.[118–121]

In the laboratory

Characterization of the morphological features of scaffolds can be used to validate a production lot, demonstrate reproducibility in industrial settings, and create guidelines for nanofiber scaffold use in a clinical setting. One example is the morphological characterization of biodegradable nanofibers as they are degraded in a physiologically relevant solution. Figure 4 shows SEM micrographs of PLGA nanofibers that have been degraded for 63 days in a medium used for growth and culture of RPE cells.

To degrade scaffolds, triplicate 1.5 mm in diameter scaffold cutouts were each placed in 1 mL of RPE growth medium and the media were changed every other day on the scaffolds for 63 days. Triplicate samples were used at each time point to ensure uniformity of degradation. Cells were not cultured with these scaffolds and thus *in vitro* effects of pH change were not assessed. These micrographs were analyzed for key morphological features of scaffolds using DiameterJ with the goal to ensure lot/batch consistency and to generate degradation kinetic data for feasibility studies of an Investigational New Drug application for the use of RPE cells in a phase I clinical trial.

The fibers shown in Fig. 4A–F were analyzed and the results can be seen in Fig. 4G–I. Analysis of the fibers was not performed after day 28 because fiber morphology had collapsed to such an extent that accurate measures of fiber diameter and porosity were no longer possible. Figure 4G–I shows a trend of fibers increasing in diameter as they degrade, and both the void size and total percent porosity of the scaffolds shrinks. This is to be expected as PLGA is a bulk degrading polymer and this trend of fiber swelling and void size decreasing has been published previously.[122]

Mechanical characterization

Mechanical characterization of nanofiber scaffolds has 2 different levels of specificity: bulk scaffold properties and single fiber mechanics. First, the bulk characterization of the nanofiber scaffold mechanical properties. These bulk

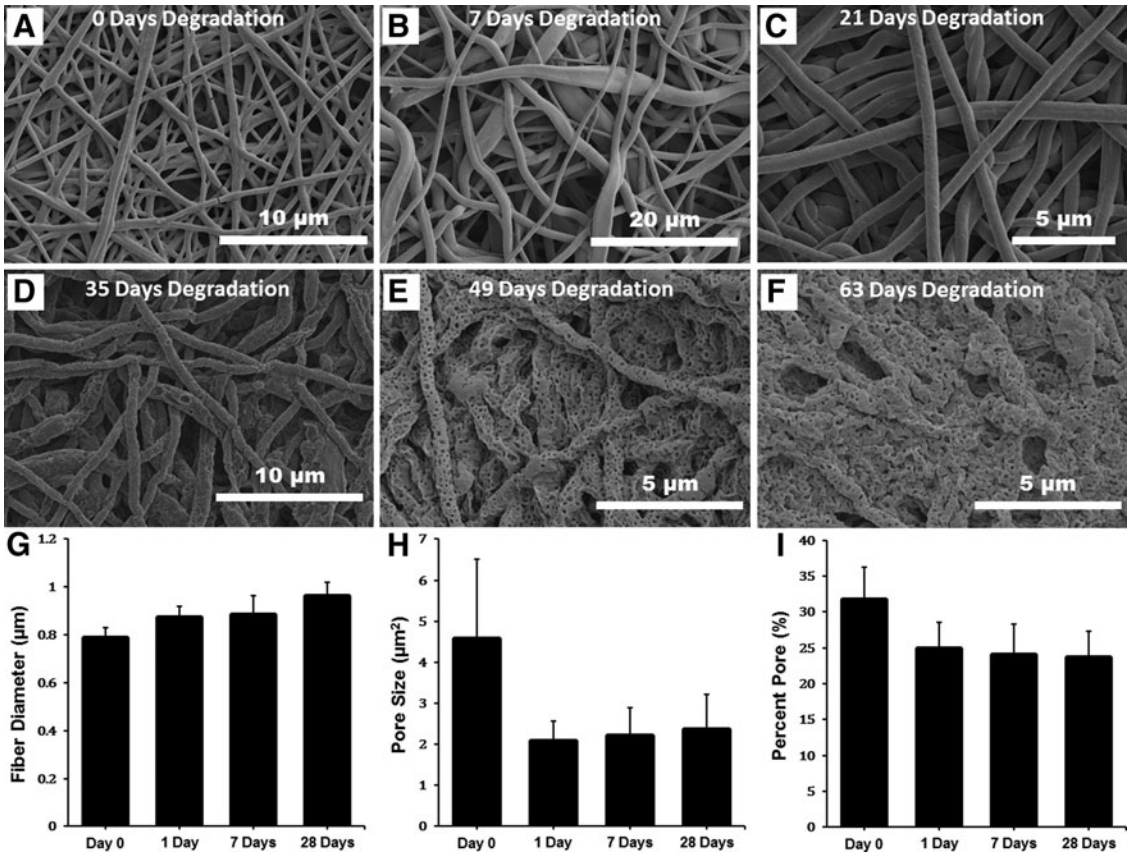

FIG. 4. Assessment of a PLGA nanofiber scaffold's morphological features as a function of time. Scanning electron micrographs of the PLGA scaffold at day 0 (before any degradation), and after 7, 21, 35, 49, and 63 days of degradation **(A–F,** respectively). Assessment of mean fiber diameter **(G)**, pore size **(H)**, and percent pore **(I)** as a function of degradation time was performed using visual analysis. No assessment after 28 days could be made due to degradation being so great that scaffold fibers could no longer be delineated.

characterization techniques involve measuring a complete nanofibrous scaffold's tensile yield strength,[123–128] toughness, ultimate tensile strength, tensile modulus,[123–128] burst pressure,[124–126] tearing strength, flexural strength,[124] and bending modulus.[129] Second, individual nanofiber mechanical properties can be measured using techniques such as atomic force microscopy and microstrain devices.[130] Differences between bulk and single nanofiber properties have been shown to vary by orders of magnitude.[128,131] Single nanofiber mechanical properties have been shown to be critical in governing cell growth, morphology, and viability.[132] However, virtually all biodegradable polyester nanofibers can be formulated to fall within the physiological range of Bruch's membrane's mechanical properties and thus will not be discussed in detail here.[133] Furthermore, for clinical applications, only bulk properties of the scaffold ultimately determine scaffold utility for handling and implantation.

Mechanical properties of nanofiber scaffolds required for optimal growth of RPE monolayer and for transplantation in the eye to the subretinal space have received little attention. A few reports have shown limited mechanical tests of scaffolds[25,133] used for growing RPE and no studies have been done to determine which mechanical properties correlate with successful cell growth, viability, functionality, and scaffold implantation. However, to expedite scaffold development, the creation of a comprehensive predictive model indicating which of these properties highly correlates with implantation success and what the minimum threshold for each of these properties for handling and implantation of the scaffolds is would be invaluable.

Cell Replacement Therapy Using an RPE Patch on a Synthetic Nanofiber Scaffold

Using the knowledge gained from the studies discussed in the Synthetic nanofibrous scaffolds section of this report and extensive experience with iPSC-derived RPE, a cell replacement therapy using a nanofiber/RPE patch was developed. During the development of this patch, several of the production techniques discussed above were compared using the testing procedures outlined in the Nanofiber Scaffold Characterization section of this report. Direct comparisons between scaffolds with different properties and these properties' relationship with cell performance were able to be assessed using the quantitative testing procedures/software discussed above. The specific outcome of these results is outside the scope of this review and is yet to be published. However, the general procedure that was used is highlighted here to provide the reader with a framework for developing their own nanofiber tissue-engineered construct.

First, biological screening tests were performed on a variety of nanofibrous materials to determine which materials supported RPE growth and function. For each of these scaffolds, the morphological properties of the scaffold were

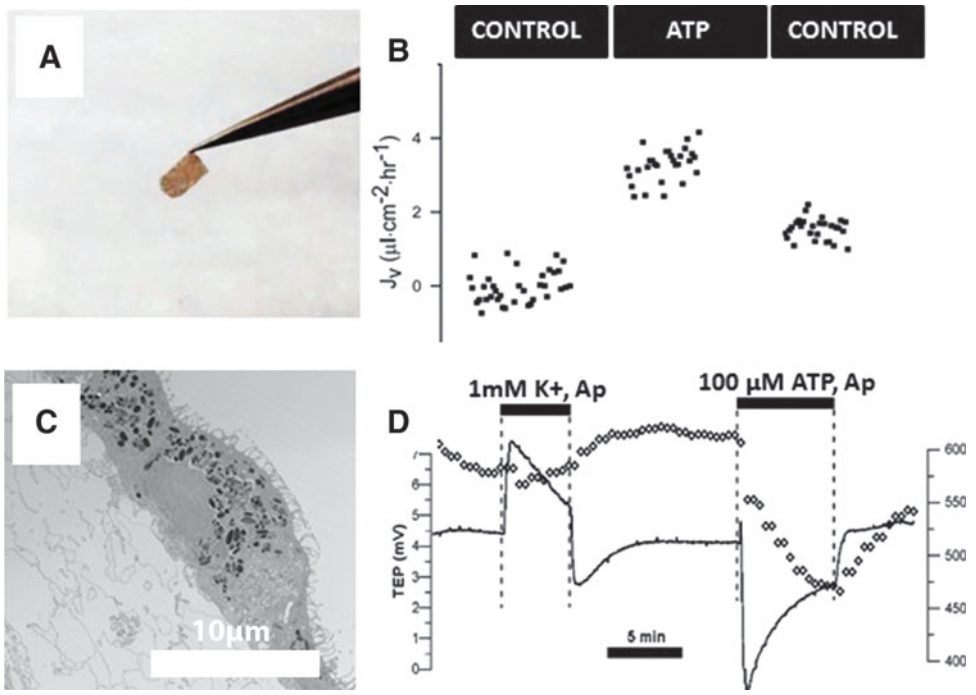

FIG. 5. iPSC-RPE cells on scaffolds. Representative figures of mature RPE monolayers on biodegradable PLGA scaffolds. Image of cell-laden implant ready for transplantation **(A)**. Transepithelial fluid transport by RPE cells in response to ATP application **(B)**. Transmission electron microscope image of RPE cells on PLGA scaffold demonstrating apical processes, apical melanosome localization, and basal infoldings in RPE cells **(C)**. Intracellular microelectrode recordings (Üssing chamber) measured RPE apical and basolateral membrane potential (V_A, V_B), TEP, total epithelial resistance (Rt), and apical-to-basal membrane resistance ratio (R_A/R_B) **(D)**. The responses to the perfusion of apical 1 mM K+ (mimicking the transition from dark to light) and ATP (candidate for light peak substrate) were recorded. All these responses of hfRPE cultured on scaffold are highly analogous to that occurring in native human RPE. TEP, transepithelial potential.

determined using the techniques discussed in the Nanofiber Scaffold Characterization section of this article. Scaffolds that showed good RPE viability and produced RPE that was hexagonal, pigmented, and in a monolayer were then compared to determine scaffold properties that led to successful RPE formulation. Next, mechanical properties of the scaffolds were assessed (as discussed in the Mechanical characterization section of this article) after degradation to determine which had the mechanical robustness to be implanted. After completing mechanical testing and eliminating scaffolds that were not mechanically robust enough, properties of scaffolds were iterated and an in-depth characterization of RPE phenotype was performed on each to fully optimize the system for maximal mechanical stability of the scaffolds with the minimum thickness necessary to promote a fully mature RPE phenotype.

Table 1. Summary Table of Scaffold Properties, Reference Sources, and Key Findings

Fiber category	*Subcategory*	*References*	*Key findings*
Material type	Natural	14,16,17,22,45–56,59	Natural or synthetic fibers support RPE growth to a statistically indistinguishable amount.
	Hybrid	15	
	Synthetic	18–20,25–27,58,59	
Scaffold structure	Nonporous membrane	15,24,25,27,58	Nanofiber scaffolds cause RPE to develop a more physiologically functional phenotype over that of nonporous membranes
	Porous membrane	12,13,28–30	
	Nanofiber scaffold	14–20,22,25–27,45–56,58,59	
Diameter	<200 nm	15,27	Nanofibers between 150 and 400 nm optimally support RPE growth and function. No direct comparisons between 150 and 400 nm scaffolds have been performed.
	200–400 nm	24,56	
	400–1,000 nm	25,56	
	>1,000 nm	18,56,57	
Surface Modification	Peptide	18	Enhancing cell adhesion through peptides, proteins, or plasma treatment increases RPE viability and functionality.
	Polymer composition	26	
	Protein	18,57	
	Plasma (O_2, N_2)	19,57	

RPE, retinal pigment epithelium.

As discussed above, coating scaffolds with biological adhesion molecules naturally found in the cell ECM (collagen, fibrinogen, vitronectin, etc.) improves RPE survival and differentiation. Thus, scaffolds were coated with xenogeneic-free human ECM proteins. These coated porous scaffolds were placed onto nondegradable porous membranes to enable substrate support on the basal side of the RPE monolayer and to allow the medium to perfuse on both the apical and basal sides of the developing monolayer. This culture system allowed the monolayer to grow in a polarized manner with prominent, apically located tight junctions that allow distinct membrane protein compartmentalization toward apical and basal sides. Additionally, the porous membrane relieved the hydrostatic pressure generated by a functional RPE, preventing fluid from accumulating in the sub-RPE space and producing unwanted liftoff of the tissue.

Validation of RPE grown *in vitro* on these nanofiber scaffolds was imperative to ensure safety and efficacy of the implanted tissue. Thus, before implantation, iPSC-derived RPE cultured on nanofibrous scaffolds was evaluated for its ability to recapitulate native RPE characteristics as discussed in the Generation and Characterization of RPE Cells section of this report. Figure 5 shows the final implantation product as well as the results of physiological tests of the RPE grown on these nanofibrous scaffolds, including morphological characteristics (Fig. 5B), fluid pumping (J_v) in response to 100 μM ATP (Fig. 5C), and transepithelial potential (TEP) (Fig. 5D). iPSC-RPE (Fig. 5B) grown on scaffolds showed an increase in fluid transport when stimulated by ATP. The ATP-induced increase in fluid transport is known to be due to the activation of P2Y2 receptors, which have been shown to respond to endogenous nucleotides. Intracellular microelectrode recordings (Ussing chamber) were used to measure iPSC-RPE TEP and total epithelial resistance (Rt) and can be seen in Fig. 5D. The responses to the perfusion of apical 1 mM K+ (mimicking the transition from dark to light) and ATP (candidate for light peak substrate) are shown. The fluid transport, cell morphology, TEP, and Rt results shown in Fig. 5C and D mimic the known characteristics of native RPE *in vivo*. Thus, RPE grown on PLGA nanofibers was deemed as a promising candidate for clinical applications.

Conclusion

The production of tissue-engineered scaffolds has seen major strides in the past 5 years. Several desirable characteristics of synthetic or naturally derived scaffolds have been identified, including 150–400 nm fiber diameter, a fiber density that is high enough to not allow cells to migrate into the scaffold so that a cell monolayer is formed on top of the scaffold, and modified fiber surface (either chemically altered or functionalized with bioadhesive proteins/peptides) to enhance cell adhesion. Table 1 shows a summary of these findings and the works from which the conclusions were drawn. Additionally, both production and assessment techniques are available to compare nanofiber scaffolds between lot-to-lot and therapy-to-therapy. These techniques have formed the framework for reproducibly generating a well-characterized, mechanically robust scaffold made from GMP-grade and xeno-free material. These kinds of scaffolds are being combined with GMP-grade and reproducible RPE differentiation protocols that generate well-characterized and functional RPE. An example was provided of a cell/scaffold construct that is currently in the process of being developed for a clinical trial, in which the above listed scaffold production and assessment techniques are being used. Moreover, recent progress from several groups[15] in the field appears to show that the development of an ideal scaffold is on the horizon and that soon a commercially viable cell replacement therapy for retinal degenerative diseases will be available.

Acknowledgments

This work was, in part, supported by NEI Intramural Funds, NIH CRM, and NIH Common Fund grants to K. Bharti. The authors would like to thank Kiel Gramley from FibeRio Technology Corporation for giving the SEM image of melt spun fibers in Fig. 3C. This article, a contribution of NIST, is not subject to US copyright. Certain equipment and instruments or materials are identified in the article to adequately specify nanofiber production capabilities. Such identification does not imply recommendation by NIH/NIST, nor does it imply that the materials are necessarily the best available for the purpose.

Author Disclosure Statement

No competing financial interests exist.

References

1. Li, R., et al. IFN{gamma} regulates retinal pigment epithelial fluid transport. *Am. J. Physiol. Cell Physiol.* 297: C1452–1465, 2009.
2. Adijanto, J., Banzon, T., Jalickee, S., Wang, N.S., and Miller, S.S. CO2-induced ion and fluid transport in human retinal pigment epithelium. *J. Gen. Physiol.* 133:603–622, 2009.
3. Quinn, R.H., Quong, J.N., and Miller, S.S. Adrenergic receptor activated ion transport in human fetal retinal pigment epithelium. *Invest. Ophthalmol. Vis. Sci.* 42:255–264, 2001.
4. Cai, X., Conley, S.M., and Naash, M.I. RPE65: role in the visual cycle, human retinal disease, and gene therapy. *Ophthalmic Genet.* 30:57–62, 2009.
5. Longbottom, R., et al. Genetic ablation of retinal pigment epithelial cells reveals the adaptive response of the epithelium and impact on photoreceptors. *Proc. Natl. Acad. Sci. U. S. A.* 106:18728–18733, 2009.
6. Busskamp, V., et al. Genetic reactivation of cone photoreceptors restores visual responses in retinitis pigmentosa. *Science.* 329:413–417, 2010.
7. Curcio, C.A., and Johnson, M. *Retina*, 5th edition. Elsevier, Inc., London, England; 2013; 1, 2564.
8. Booij, J.C., Baas, D.C., Beisekeeva, J., Gorgels, T.G.M.F., and Bergen, A.A. The dynamic nature of Bruch's membrane. *Prog. Retin. Eye Res.* 29:1–18, 2564.
9. Miller, S.S., and Edelman, J.L. Active ion transport pathways in the bovine retinal pigment epithelium. *J. Physiol.* 424:283–300, 1990.
10. Shi, G., et al. Control of chemokine gradients by the retinal pigment epithelium. *Invest. Ophthalmol. Vis. Sci.* 49:4620–4630, 2008.
11. Maminishkis, A., et al. Confluent monolayers of cultured human fetal retinal pigment epithelium exhibit morphol-

ogy and physiology of native tissue. *Invest. Ophthalmol. Vis. Sci.* 47:3612–3624, 2006.
12. Diniz, B., et al. Subretinal implantation of retinal pigment epithelial cells derived from human embryonic stem cells: improved survival when implanted as a monolayer. *Invest. Ophthalmol. Vis. Sci.* 54:5087–5096, 2013.
13. Stanzel, B.V., et al. Human RPE stem cells grown into polarized RPE monolayers on a polyester matrix are maintained after grafting into rabbit subretinal space. *Stem Cell Rep.* 2:64–77, 2014.
14. Singh, S., Woerly, S., and McLaughlin, B.J. Natural and artificial substrates for retinal pigment epithelial monolayer transplantation. *Biomaterials.* 22:3337–3343, 2001.
15. Jha, B.S., and Bharti, K. Regenerating retinal pigment epithelial cells to cure blindness: a road towards personalized artificial tissue. *Curr. Stem Cell Rep.* 1:79–91, 2015.
16. Xiang, P., et al. A novel Bruch's membrane-mimetic electrospun substrate scaffold for human retinal pigment epithelium cells. *Biomaterials.* 35:9777–9788, 2014.
17. Gonçalves, S., et al. Bacterial Cellulose As a Support for the growth of retinal pigment epithelium. *Biomacromolecules.* 16:1341–1351, 2015.
18. Sorkio, A.E., et al. Biomimetic collagen I and IV double layer Langmuir–Schaefer films as microenvironment for human pluripotent stem cell derived retinal pigment epithelial cells. *Biomaterials.* 51:257–269, 2015.
19. Treharne, A.J., Thomson, H.A.J., Grossel, M.C., and Lotery, A.J. Developing methacrylate-based copolymers as an artificial Bruch's membrane substitute. *J. Biomed. Mater. Res. A.* 100A:2358–2364, 2012.
20. Krishna, Y., et al. Expanded polytetrafluoroethylene as a substrate for retinal pigment epithelial cell growth and transplantation in age-related macular degeneration. *Br. J. Ophthalmol.* 95:569–573, 2011.
21. Da Silva, G.R., et al. In vitro and in vivo ocular biocompatibility of electrospun poly(ε-caprolactone) nanofibers. *Eur. J. Pharm. Sci.* 73:9–19, 2015.
22. Wang, H., Ninomiya, Y., Sugino, I.K., and Zarbin, M.A. Retinal pigment epithelium wound healing in human Bruch's membrane explants. *Invest. Ophthalmol. Vis. Sci.* 44:2199–2210, 2003.
23. Lu, B., Zhu, D., Hinton, D., Humayun, M.S., and Tai, Y.-C. Mesh-supported submicron parylene-C membranes for culturing retinal pigment epithelial cells. *Biomed. Microdevices.* 14:659–667, 2012.
24. Warnke, P.H., et al. Primordium of an artificial Bruch's membrane made of nanofibers for engineering of retinal pigment epithelium cell monolayers. *Acta Biomater.* 9:9414–9422, 2013.
25. Popelka, Š., et al. A frame-supported ultrathin electrospun polymer membrane for transplantation of retinal pigment epithelial cells. *Biomed. Mater.* 10:045022, 2015.
26. Thomson, H.A.J., Treharne, A.J., Walker, P., Grossel, M.C., and Lotery, A.J. Optimisation of polymer scaffolds for retinal pigment epithelium (RPE) cell transplantation. *Br. J. Ophthalmol.* 95:563–568, 2011.
27. Thieltges, F., Stanzel, B.V., Liu, Z., and Holz, F.G. A nanofibrillar surface promotes superior growth characteristics in cultured human retinal pigment epithelium. *Ophthalmic Res.* 46:133–140, 2011.
28. Carr, A.-J.F., et al. Development of human embryonic stem cell therapies for age-related macular degeneration. *Trends Neurosci.* 36:385–395, 2013.
29. McHugh, K.J., Tao, S.L., and Saint-Geniez, M. Porous poly(ε-caprolactone) scaffolds for retinal pigment epithelium transplantation. *Invest. Ophthalmol. Vis. Sci.* 55: 1754–1762, 2014.
30. Li, L.X., and Turner, J.E. Inherited retinal dystrophy in the RCS rat: prevention of photoreceptor degeneration by pigment epithelial cell transplantation. *Exp. Eye Res.* 47: 911–917, 1988.
31. van Zeeburg, E.J.T., Maaijwee, K.J.M., Missotten, T.O.A.R., Heimann, H., and van Meurs, J.C. A free retinal pigment epithelium-choroid graft in patients with exudative age-related macular degeneration: results up to 7 years. *Am. J. Ophthalmol.* 153:120–127.e2, 2012.
32. Buchholz, D.E., et al. Rapid and efficient directed differentiation of human pluripotent stem cells into retinal pigmented epithelium. *Stem Cells Transl. Med.* 2:384–393, 2013.
33. Buchholz, D.E., et al. Derivation of functional retinal pigmented epithelium from induced pluripotent stem cells. *Stem Cells* 27:2427–2434, 2009.
34. Perkel, J.M. Disease modeling with patient-specific iPS cells. *Science.* 347:1271–1273, 2015.
35. Ferrer, M., et al. A multiplex high-throughput gene expression assay to simultaneously detect disease and functional markers in induced pluripotent stem cell-derived retinal pigment epithelium. *Stem Cells Transl. Med.* 3:911–922, 2014.
36. Chambers, S.M., et al. Highly efficient neural conversion of human ES and iPS cells by dual inhibition of SMAD signaling. *Nat. Biotechnol.* 27:275–280, 2009.
37. Maminishkis, A., and Miller, S.S. Experimental models for study of retinal pigment epithelial physiology and pathophysiology. *J. Vis. Exp.* (45). pii: 2032, 2010; DOI:10.3791/2032
38. Rizzolo, L.J. Barrier properties of cultured retinal pigment epithelium. *Exp. Eye Res.* 126:16–26, 2014.
39. Liao, J.-L., et al. Molecular signature of primary retinal pigment epithelium and stem-cell-derived RPE cells. *Hum. Mol. Genet.* 19:4229–4238, 2010.
40. Bharti, K., et al. A regulatory loop involving PAX6, MITF, and WNT signaling controls retinal pigment epithelium development. *PLoS Genet.* 8:e1002757, 2012.
41. Capowski, E.E., et al. Loss of MITF expression during human embryonic stem cell differentiation disrupts retinal pigment epithelium development and optic vesicle cell proliferation. *Hum. Mol. Genet.* 23:6332–6344, 2014.
42. Bharti, K., Miller, S.S., and Arnheiter, H. The new paradigm: retinal pigment epithelium cells generated from embryonic or induced pluripotent stem cells. *Pigment Cell Melanoma Res.* 24:21–34, 2011.
43. Gullapalli, V.K., Sugino, I.K., Van Patten, Y., Shah, S., and Zarbin, M.A. Impaired RPE survival on aged submacular human Bruch's membrane. *Exp. Eye Res.* 80:235–248, 2005.
44. Tezel, T.H., Kaplan, H.J., and Del Priore, L.V. Fate of human retinal pigment epithelial cells seeded onto layers of human Bruch's membrane. *Invest. Ophthalmol. Vis. Sci.* 40:467–476, 1999.
45. Sugino, I.K., et al. Comparison of FRPE and human embryonic stem cell–derived RPE behavior on aged human Bruch's membrane. *Invest. Ophthalmol. Vis. Sci.* 52:4979–4997, 2011.
46. Tezel, T.H., Del Priore, L.V., and Kaplan, H.J. Reengineering of aged Bruch's membrane to enhance retinal pigment epithelium repopulation. *Invest. Ophthalmol. Vis. Sci.* 45:3337–3348, 2004.
47. Tezel, T.H., and Priore, L.V.D. Repopulation of different layers of host human Bruch's membrane by retinal pigment epithelial cell grafts. *Invest. Ophthalmol. Vis. Sci.* 40:767–774, 1999.

48. Del Priore, L.V., Geng, L., Tezel, T.H., and Kaplan, H.J. Extracellular matrix ligands promote RPE attachment to inner Bruch's membrane. *Curr. Eye Res.* 25:79–89, 2002.
49. Sugino, I.K., et al. Cell-deposited matrix improves retinal pigment epithelium survival on aged submacular human Bruch's membrane. *Invest. Ophthalmol. Vis. Sci.* 52:1345–1358, 2011.
50. Sugino, I.K., et al. A method to enhance cell survival on Bruch's membrane in eyes affected by age and age-related macular degeneration. *Invest. Ophthalmol. Vis. Sci.* 52: 9598–9609, 2011.
51. Vemuganti, G., and Singhal, S. Primary adult human retinal pigment epithelial cell cultures on human amniotic membranes. *Indian J. Ophthalmol.* 53:109, 2005.
52. Akrami, H., et al. Evaluation of RPE65, CRALBP, VEGF, CD68, and tyrosinase gene expression in human retinal pigment epithelial cells cultured on amniotic membrane. *Biochem. Genet.* 49:313–322, 2011.
53. Ohno-Matsui, K., et al. The effects of amniotic membrane on retinal pigment epithelial cell differentiation. *Mol. Vis.* 11:1–10, 2005.
54. Capeáns, C., et al. Amniotic membrane as support for human retinal pigment epithelium (RPE) cell growth. *Acta Ophthalmol. Scand.* 81:271–277, 2003.
55. Stanzel, B.V., et al. Amniotic membrane maintains the phenotype of rabbit retinal pigment epithelial cells in culture. *Exp. Eye Res.* 80:103–112, 2005.
56. Lee, C.J., et al. Microcontact printing on human tissue for retinal cell transplantation. *Arch. Ophthalmol.* 120:1714–1718, 2002.
57. Wolf, K., et al. Collagen-based cell migration models in vitro and in vivo. *Semin. Cell Dev. Biol.* 20:931–941, 2009.
58. Liu, Z., Yu, N., Holz, F.G., Yang, F., and Stanzel, B.V. Enhancement of retinal pigment epithelial culture characteristics and subretinal space tolerance of scaffolds with 200 nm fiber topography. *Biomaterials.* 35:2837–2850, 2014.
59. Sorkio, A., et al. Surface modified biodegradable electrospun membranes as a carrier for human embryonic stem cell-derived retinal pigment epithelial cells. *Tissue Eng. Part A.* 21:2301–2314, 2015.
60. Luo, C.J., Stoyanov, S.D., Stride, E., Pelan, E., and Edirisinghe, M. Electrospinning versus fibre production methods: from specifics to technological convergence. *Chem. Soc. Rev.* 41:4708–4735, 2012.
61. Persano, L., Camposeo, A., Tekmen, C., and Pisignano, D. Industrial upscaling of electrospinning and applications of polymer nanofibers: a review. *Macromol. Mater. Eng.* 298:504–520, 2013.
62. Stanger, J.J., Tucker, N., Buunk, N., and Truong, Y.B. A comparison of automated and manual techniques for measurement of electrospun fibre diameter. *Polym. Test.* 40:4–12, 2014.
63. Hotaling, N.A., Bharti, K., Kriel, H., and Simon Jr., C.G., and Diameter, J. A validated open source nanofiber diameter measurement tool. *Biomaterials.* 61:327–338, 2015.
64. Blackwood, K.A., et al. Development of biodegradable electrospun scaffolds for dermal replacement. *Biomaterials.* 29:3091–3104, 2008.
65. Albrecht, D.R., Underhill, G.H., Mendelson, A., and Bhatia, S.N. Multiphase electropatterning of cells and biomaterials. *Lab. Chip.* 7:702–709, 2007.
66. Kim, S.-E., et al. Surface modification of melt extruded poly(ε-caprolactone) nanofibers: toward a new scalable biomaterial scaffold. *ACS Macro Lett.* 3:585–589, 2014.
67. Zuo, F., et al. Nanofibers from melt blown fiber-in-fiber polymer blends. *ACS Macro Lett.* 2:301–305, 2013.
68. Behrens, A.M., et al. In situ deposition of PLGA nanofibers via solution blow spinning. *ACS Macro Lett.* 3:249–254, 2014.
69. Zelenski, C.M., and Dorhout, P.K. Template synthesis of near-monodisperse1 microscale nanofibers and nanotubules of MoS2. *J. Am. Chem. Soc.* 120:734–742, 1998.
70. Che, G., Lakshmi, B.B., Martin, C.R., Fisher, E.R., and Ruoff, R.S. Chemical vapor deposition based synthesis of carbon nanotubes and nanofibers using a template method. *Chem. Mater.* 10:260–267, 1998.
71. Badrossamay, M.R., McIlwee, H.A., Goss, J.A., and Parker, K.K. Nanofiber assembly by rotary jet-spinning. *Nano Lett.* 10:2257–2261, 2010.
72. Capadona, J.R., et al. A versatile approach for the processing of polymer nanocomposites with self-assembled nanofibre templates. *Nat. Nanotechnol.* 2:765–769, 2007.
73. Hartgerink, J.D., Beniash, E., and Stupp, S.I. Self-assembly and mineralization of peptide-amphiphile nanofibers. *Science.* 294:1684–1688, 2001.
74. Subbiah, T., Bhat, G.S., Tock, R.W., Parameswaran, S., and Ramkumar, S.S. Electrospinning of nanofibers. *J. Appl. Polym. Sci.* 96:557–569, 2005.
75. Kong, L., and Ziegler, G.R. Quantitative relationship between electrospinning parameters and starch fiber diameter. *Carbohydr. Polym.* 92:1416–1422, 2013.
76. Khanlou, H.M., et al. Prediction and optimization of electrospinning parameters for polymethyl methacrylate nanofiber fabrication using response surface methodology and artificial neural networks. *Neural Comput. Appl.* 25: 767–777, 2014.
77. Hernández-Vargas, J., González-Campos, J.B., Lara-Romero, J., and Ponce-Ortega, J.M. A mathematical programming approach for the optimal synthesis of nanofibers through an electrospinning process. *ACS Sustain. Chem. Eng.* 2:454–464, 2014.
78. Faridi-Majidi, R., Ziyadi, H., Naderi, N., and Amani, A. Use of artificial neural networks to determine parameters controlling the nanofibers diameter in electrospinning of nylon-6,6. *J. Appl. Polym. Sci.* 124:1589–1597, 2012.
79. Essalhi, M., Cojocaru, C., Garcĺa-Payo, M.C., and Arribas, P. Response surface modeling and optimization of electrospun nanofiber membranes. *Open Nanosci. J.* 7:8–17, 2013.
80. Tomaszewski, W., and Szadkowski, M. Investigation of electrospinning with the use of a multi-jet electrospinning head. *Fibers Text. East. Eur.* 13:22–26, 2005.
81. Varesano, A., Rombaldoni, F., Mazzuchetti, G., Tonin, C., and Comotto, R. Multi-jet nozzle electrospinning on textile substrates: observations on process and nanofibre mat deposition. *Polym. Int.* 59:1606–1615, 2010.
82. Wang, X., Niu, H., Lin, T., and Wang, X. Needleless electrospinning of nanofibers with a conical wire coil. *Polym. Eng. Sci.* 49:1582–1586, 2009.
83. Kostakova, E., Meszaros, L., and Gregr, J. Composite nanofibers produced by modified needleless electrospinning. *Mater. Lett.* 63:2419–2422, 2009.
84. Niu, H., Lin, T., and Wang, X. Needleless electrospinning. I. A comparison of cylinder and disk nozzles. *J. Appl. Polym. Sci.* 114:3524–3530, 2009.
85. snc-fibers. Available at www.sncfibers.com/ (accessed 17th August 2015).

86. Mellado, P., et al. A simple model for nanofiber formation by rotary jet-spinning. *Appl. Phys. Lett.* 99:203107, 2011.
87. Gupta, B., Revagade, N., Anjum, N., Atthoff, B., and Hilborn, J. Preparation of poly(lactic acid) fiber by dry–jet–wet spinning. II. Effect of process parameters on fiber properties. *J. Appl. Polym. Sci.* 101:3774–3780, 2006.
88. FibeRio Technology Corporation. Basic research. Available at http://fiberiotech.com/products/rd-equipment/basic-research/ (accessed 17th August 2015).
89. Sarkar, K., et al. Electrospinning to Forcespinning™. *Mater. Today.* 13:12–14, 2010.
90. Bilbao-Sainz, C., et al. Solution blow spun poly(lactic acid)/hydroxypropyl methylcellulose nanofibers with antimicrobial properties. *Eur. Polym. J.* 54:1–10, 2014.
91. Oliveira, J.E., et al. Nano and submicrometric fibers of poly(D,L-lactide) obtained by solution blow spinning: process and solution variables. *J. Appl. Polym. Sci.* 122: 3396–3405, 2011.
92. Medeiros, E.S., Glenn, G.M., Klamczynski, A.P., Orts, W.J., and Mattoso, L.H.C. Solution blow spinning: a new method to produce micro- and nanofibers from polymer solutions. *J. Appl. Polym. Sci.* 113:2322–2330, 2009.
93. Gupta, V., and Kothari, V. *Manufactured Fibre Technology.* Netherlands*:* V.B. Gupta | Springer, London, England, 1997.
94. Tutak, W., et al. The support of bone marrow stromal cell differentiation by airbrushed nanofiber scaffolds. *Biomaterials.* 34:2389–2398, 2013.
95. Gupta, B., Revagade, N., and Hilborn, J. In vitro degradation of dry-jet-wet spun poly(lactic acid) monofilament and knitted scaffold. *J. Appl. Polym. Sci.* 103:2006–2012, 2007.
96. Gupta, B., Revagade, N., and Hilborn, J. Poly(lactic acid) fiber: an overview. *Prog. Polym. Sci.* 32:455–482, 2007.
97. Gangwal, S., and Wright, M. Nanofibres: New scalable technology platform for producing polymeric nanofibres. *Filtr. Sep.* 50:30–33, 2013.
98. Velev, O.D., and Alargova, R.G. Process for preparing microrods using liquid-liquid dispersion. U.S. Patent 7323540 B2. January 29, 2008.
99. Technology | Xanofi. Available at http://xanofi.com/technology/ (accessed 17th August 2015).
100. ISO 9073-5:2008. *Textiles—Test Methods for Nonwovens—Part 5: Determination of Resistance to Mechanical Penetration (Ball Burst Procedure).* ISO, Geneva, Switzerland, 2012.
101. ISO 9073-4:1997. *Textiles—Test Methods for Nonwovens—Part 4: Determination of Tear Resistance*. ISO, 2013.
102. ISO 9073-3:1989. *Textiles—Test Methods for Nonwovens—Part 3: Determination of Tensile Strength and Elongation*. ISO, 2015.
103. Fiji Is Just ImageJ. Available at http://fiji.sc/wiki/index.php/Fiji (accessed 28th July 2014).
104. Schindelin, J., et al. Fiji: an open-source platform for biological-image analysis. *Nat. Methods.* 9:676–682, 2012.
105. ImageJ. Available at http://imagej.nih.gov/ij/index.html (accessed 28th July 2014).
106. Rezakhaniha, R., et al. Experimental investigation of collagen waviness and orientation in the arterial adventitia using confocal laser scanning microscopy. *Biomech. Model. Mechanobiol.* 11:461–473, 2012.
107. Woolley, A.J., Desai, H.A., Steckbeck, M.A., Patel, N.K., and Otto, K.J. In situ characterization of the brain–microdevice interface using device capture histology. *J. Neurosci. Methods.* 201:67–77, 2011.
108. Liu, Z.Q. Scale space approach to directional analysis of images. *Appl. Opt.* 30:1369–1373, 1991.
109. Schaub, N.J., Kirkpatrick, S.J., and Gilbert, R.J. Automated methods to determine electrospun fiber alignment and diameter using the radon transform. *BioNanoScience.* 3:329–342, 2013.
110. D'Amore, A., Stella, J.A., Wagner, W.R., and Sacks, M.S. Characterization of the complete fiber network topology of planar fibrous tissues and scaffolds. *Biomaterials.* 31:5345–5354, 2010.
111. Tomba, E., et al. Artificial vision system for the automatic measurement of interfiber pore characteristics and fiber diameter distribution in nanofiber assemblies. *Ind. Eng. Chem. Res.* 49:2957–2968, 2010.
112. Igathinathane, C., Pordesimo, L.O., and Batchelor, W.D. Major orthogonal dimensions measurement of food grains by machine vision using ImageJ. *Food Res. Int.* 42:76–84, 2009.
113. Igathinathane, C., Pordesimo, L.O., Columbus, E.P., Batchelor, W.D., and Methuku, S.R. Shape identification and particles size distribution from basic shape parameters using ImageJ. *Comput. Electron. Agric.* 63:168–182, 2008.
114. Papadopulos, F., et al. Common tasks in microscopic and ultrastructural image analysis using ImageJ. *Ultrastruct. Pathol.* 31:401–407, 2007.
115. Murphy, M.M., Lawson, J.A., Mathew, S.J., Hutcheson, D.A., and Kardon, G. Satellite cells, connective tissue fibroblasts and their interactions are crucial for muscle regeneration. *Development.* 138:3625–3637, 2011.
116. Ziabari, M., Mottaghitalab, V., and Haghi, A.K. Application of direct tracking method for measuring electrospun nanofiber diameter. *Braz. J. Chem. Eng.* 26:53–62, 2009.
117. Allahkarami, M., Bandla, S., Winarski, R.P., and Hanan, J.C. X-ray nanotomography of a nanofiber: quantitative measurement of diameter fluctuations. *Appl. Surf. Sci.* 297:9–15, 2014.
118. Širc, J., et al. Morphological characterization of nanofibers: methods and application in practice. *J. Nanomater.* 2012:e327369, 2012.
119. Ritter, H.L., and Drake, L.C. Pressure porosimeter and determination of complete macropore-size distributions. *Ind. Eng. Chem. Anal. Ed.* 17:782–786, 1945.
120. Ryu, Y.J., Kim, H.Y., Lee, K.H., Park, H.C., and Lee, D.R. Transport properties of electrospun nylon 6 nonwoven mats. *Eur. Polym. J.* 39:1883–1889, 2003.
121. Zhang, Z., et al. Polyacrylonitrile and carbon nanofibers with controllable nanoporous structures by electrospinning. *Macromol. Mater. Eng.* 294:673–678, 2009.
122. Kim, K., et al. Control of degradation rate and hydrophilicity in electrospun non-woven poly(d,l-lactide) nanofiber scaffolds for biomedical applications. *Biomaterials.* 24: 4977–4985, 2003.
123. Katz, A.R., and Turner, R.J. Evaluation of tensile and absorption properties of polyglycolic acid sutures. *Surg. Gynecol. Obstet.* 131:701–716, 1970.
124. Lee, S.J., et al. The use of thermal treatments to enhance the mechanical properties of electrospun poly(ε-caprolactone) scaffolds. *Biomaterials.* 29:1422–1430, 2008.
125. Drilling, S., Gaumer, J., and Lannutti, J. Fabrication of burst pressure competent vascular grafts via electrospin-

ning: effects of microstructure. *J. Biomed. Mater. Res. A.* 88A:923–934, 2009.
126. Lee, S.J., et al. Development of a composite vascular scaffolding system that withstands physiological vascular conditions. *Biomaterials.* 29:2891–2898, 2008.
127. Wu, L., and Ding, J. In vitro degradation of three-dimensional porous poly(d,l-lactide-co-glycolide) scaffolds for tissue engineering. *Biomaterials.* 25:5821–5830, 2004.
128. Yao, J., Bastiaansen, C.W.M., and Peijs, T. High strength and high modulus electrospun nanofibers. *Fibers.* 2:158–186, 2014.
129. Amoroso, N.J., et al. Microstructural manipulation of electrospun scaffolds for specific bending stiffness for heart valve tissue engineering. *Acta Biomater.* 8:4268–4277, 2012.
130. Tan, E.P.S., and Lim, C.T. Mechanical characterization of nanofibers—a review. *Compos. Sci. Technol.* 66:1102–1111, 2006.
131. Croisier, F., et al. Mechanical testing of electrospun PCL fibers. *Acta Biomater.* 8:218–224, 2012.
132. Vogel, V., and Sheetz, M. Local force and geometry sensing regulate cell functions. *Nat. Rev. Mol. Cell Biol.* 7:265–275, 2006.
133. Hynes, S.R., and Lavik, E.B. A tissue-engineered approach toward retinal repair: scaffolds for cell transplantation to the subretinal space. *Graefes Arch. Clin. Exp.* 248:763–778, 2010.

Received: December 11, 2015
Accepted: March 24, 2016

Address correspondence to:
Dr. Nathan A. Hotaling
Unit on Ocular and Stem Cell Translational Research
National Eye Institute
National Institutes of Health
10 Center Drive, Building 10 Room 10B10
Bethesda, MD 20892

E-mail: nathan.Hotaling@nih.gov

Dr. Kapil Bharti
Unit on Ocular and Stem Cell Translational Research
National Eye Institute
National Institutes of Health
10 Center Drive, Building 10 Room 10B10
Bethesda, MD 20892

E-mail: kapilbharti@nei.nih.gov